



ELSEVIER

Journal of Magnetism and Magnetic Materials 214 (2000) 204–216



www.elsevier.com/locate/jmmm

Dynamic magnetization observations and reversal mechanisms of sintered and die-upset Nd–Fe–B magnets

V.V. Volkov*, Y. Zhu

Department of Applied Science, Brookhaven National Laboratory, Bldg. 480, Upton, NY 11973, USA

Received 5 November 1999; received in revised form 25 February 2000

Abstract

In situ TEM magnetizing experiments combined with Lorentz microscopy in Fresnel and Foucault mode were used to study local features of magnetization reversal in polycrystalline sintered and die-upset Nd–Fe–B magnets. The die-upset (DU) magnets featured well-aligned grain texture along the *c*-axis, while the sintered (SI) magnets have a much wider distribution of grain orientations. Despite the similarity of the hysteresis curves, we found their nanoscale behavior of the magnetization reversal was quite different. The predominant mechanism controlling reversal in DU-magnets was nucleation of reversed domains, preferentially at misaligned grain interfaces, followed by domain wall pinning at grain boundaries. In contrast, magnetization reversal in SI-magnet progressed first by nucleation and expansion of reversed domain dipoles predominantly in misaligned grains at a high magnetic field, and then by the major irreversible process via nucleation and splitting of magnetic domains near the grain boundaries of well-aligned grains at more negative fields. This process is completed with lateral expansion of newly created domain walls. A simple model for the strong pinning–trapping centers observed in DU-magnets is discussed. © 2000 Elsevier Science B.V. All rights reserved.

PACS: 75.60.Ch; 75.60.Gm; 75.70.Kw; 81.20.Ev

Keywords: Mechanisms of magnetization reversal; In situ Lorentz microscopy; Magnetic domains; Die-upset magnets; Sintered magnets

1. Introduction

Nd–Fe–B hard magnets have been used for a wide variety of applications ranging from generators, to motors and computer devices, and the market for them is growing rapidly as their properties and cost-effectiveness are improved. The magnetic properties of these magnets are controlled by

their microstructure via different materials-processing techniques. One of the most important and microstructure-sensitive parameters of a magnet is its coercive field, H_c . The formal definition of the coercivity is the intersection point of the magnetization curve $I(H_c) = 0$ with the abscissa (H -axis) at a certain negative field $H = H_c < 0$. In practice, only this parameter is used to describe how ‘hard’ a magnet is and to what critical field it can be exploited in its applications. Another approach is to define the coercive field as the point at which the maximum of magnetization gradient or magnetic susceptibility is reached. However, these

* Corresponding author. Tel.: +1-631-344-7355; fax: +1-631-344-4071.

E-mail address: volkov@sun2.bnl.gov (V.V. Volkov).

parameters alone, are not adequate to understand how the phenomenon of coercivity is related to the microstructure of a hard magnet. The reasons for this are as follows. First, the experimental data reported in the literature as well as our own results indicate that reversal of magnetization may be a complex multi-step process, possibly ruled by different mechanisms [1,2]. The mechanism may be sensitive to details of microstructure of the magnetic material, such as grain sizes, grain boundaries misorientation and secondary phases, and even to the strength of the applied field. For this reason understanding the controlling factor that determines the coercivity becomes a central research issue in improving the properties of hard magnets. The second aspect is that, in general, the polycrystalline structure of a hard magnet is often evaluated by the distribution of its grain orientations and sizes. Therefore, the local threshold fields (H_{loc}) for magnetization reversal in each grain will be a function of the amplitude and direction of the applied field, and may be very different from the H_c value defined above. Hence, the value of H_c is only a volume averaged or integrated 'figure of merit' term for a hard magnet.

In order to get more direct insight on the mechanisms of magnetization reversal, direct observation and analysis of local magnetic structure that can monitor individual magnetic domains in real time under varied applied fields is crucial. One unique approach is the use of advanced Lorentz microscopy, both in Fresnel and Foucault imaging modes, combined with in situ magnetizing experiments in a magnetic-field-characterized transmission electron microscope (TEM).

The purpose of our present work is to demonstrate how such an approach reveals fine details of magnetization reversal in Nd–Fe–B die-upset (DU) and sintered (SI) hard magnets. We believe that dynamic magnetic image analysis, combined with the conventional TEM characterization of local areas can yield a better understanding on how microstructure and structural defects might be related to coercivity of the Nd–Fe–B hard magnets. Nevertheless, like any TEM experiments, caution should be taken in extrapolating the observations. Since a TEM sample must be thin enough to be electron-beam transparent, the balance of

exchange, anisotropic and magnetostatic energy in a thin TEM-sample can differ from that in a bulk magnet. Consequently, certain parameters used to describe the structure of a magnetic domain, such as domain width and local nucleation or pinning fields H_{loc} , in thin and bulk samples may not be the same. However, these differences do not overrule the results of TEM observations for thin samples, but may change some quantitative aspects in applying the observations to the bulk.

2. Experimental

Two types of hard anisotropic magnets were used in the present study: die-upset (DU) $\text{Nd}_{13.75}\text{Fe}_{80.25}\text{B}_6$ and sintered (SI) $\text{Nd}_{15}\text{Fe}_{78.5}\text{B}_{6.5}$ permanent magnets. The nominal compositions of both samples had a slight excess of Nd over the stoichiometry of the $\text{Nd}_2\text{Fe}_{14}\text{B}$ (or $\text{Nd}_{11.43}\text{Fe}_{80}\text{B}_{5.7}$) magnetic phase, and both magnets had high-energy products. For instance, superior quality DU-magnet had an energy product of $(BH)_{\max} = 36.38$ MGOe, and remanence $B_r = 12.9$ kG. The die-upset (DU) magnets were produced at the General Motors Research and Development Center. The sintered (SI) magnets were made at Carnegie Mellon University. In some cases specified below we used better quality SI-magnets of the same composition produced by Sumitomo Special Metals Inc.

The DU-magnets were prepared from overquenched ribbons using the melt-spinning technique followed by a hot-pressing [3] and die-upsetting procedure [4,5]. The latter process is used to develop a strongly anisotropic magnet by uniaxial plastic deformation of the sample in a closed-die at about 750–800°C, which gives a strong crystallographic texture in the magnet with grain c -axis parallel to the compression direction. Usually, an applied pressure of ~ 10 kpsi for a few seconds at 750°C is sufficient to cause 50% plastic deformation [4]. More details on preparing and characterization of DU-magnets is given in Ref. [6].

Alloys for SI-magnets were prepared by arc-melting under an argon gas atmosphere, as described in Refs. [7,8]. The buttons of ingots were crashed and ball-milled for 2 h to ensure a uniform grain distribution of 3–6 μm in size. Then, the

powder grains were magnetically aligned and pressed in field of 1 T. Finally, the pressed powders were sintered in vacuum for 1 h at about 1080°C followed by annealing at 650°C for 1 h and then cooled rapidly in a cooling chamber. Similar to DU-case such a process develops a strong crystallographic texture in SI magnets and increases their energy product $(BH)_{\max}$.

Thin disk specimens for TEM observation were cut from buttons of the SI and DU magnets. Both plan-view and cross-section cut samples with its surface transverse and longitudinal to press direction, respectively, were made. The thin slices were then mechanically polished and ion-milled until perforation occurred. In situ magnetizing experiments were carried out on JEM 2000FX and JEM 3000F field-emission microscopes, operating at 200 and 300 kV, respectively. The local composition of grain interiors, grain boundaries (GB) and of secondary-phase inclusions was analyzed using the energy dispersive X-ray spectroscopy (EDS) system attached to the microscopes.

For in situ TEM experiments, all magnetic sensitive images were acquired under the free-lens-control mode. The main objective lens of the microscope was either turned off, or slightly exited to magnetize the TEM specimen, located in the bore of the objective lens pole-piece, with external field $0.02 \leq \mu_0 H_{\text{ext}} \leq 2$ T. The sample was tilted in the holder by up to $|\theta_{\max}| \leq 30^\circ$ out of the observation plane in order to apply a known in-specimen plane magnetic field $B_{\parallel} = \mu_0 H_{\text{ext}} \sin \theta$, allowing remagnetization process to be followed in situ through the hysteresis cycles. The maximum objective lens field did not exceed 3 T, however, the real-time observations of magnetic domains were possible only at $\mu_0 H_{\text{ext}} \leq 1.5$ T. The calibration of magnetic field ($\mu_0 H_{\text{ext}}$) in a sample area versus objective lens potential (U) for JEOL 3000FEG microscope was carried out by two independent methods. In first case, the external field was carefully calibrated by using a $\text{Nd}_2\text{Fe}_{14}\text{B}$ test sample measured with a superconducting quantum interference device (SQUID) magnetometer following a procedure described in Ref. [9]. In second case, we used direct Hall probe measurements with a BELL610 gaussmeter [10]. The results of both procedures agreed well within the experimental errors.

3. Results

3.1. Domain structure, microstructure and grain alignment

Conventional TEM/EDS analysis of SI and DU magnets showed that they consist of mainly hard magnetic $\text{Nd}_2\text{Fe}_{14}\text{B}$ (2–14–1) phase and some amount of submicron-size inclusions of Nd-enriched secondary phases. However, the details of their microstructure were found to be quite different.

In case of SI-magnets such inclusions were found to concentrate predominantly at the triple junction points of polygonal grains of 2–14–1 phase. The grains of hard magnetic phase did not exceed 1.5–8 μm in size and were aligned with c -axis preferably along the common easy magnetic direction of the SI-magnet. Our TEM/EDS conclusions are consistent with a plan-view image of SI-magnet (Fig. 1), taken with back-scattered electrons (BSE) in scanning electron microscope (SEM). Here, the impurity inclusions of Nd-rich secondary phases

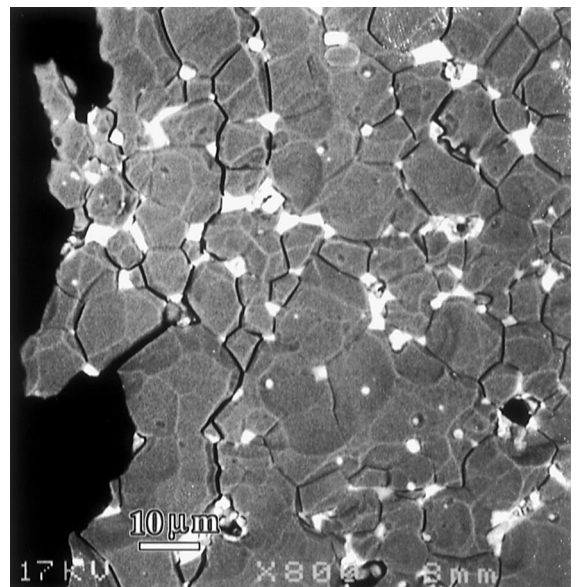


Fig. 1. SEM image of the surface of a SI-magnet sample taken with back-scattered electrons. Nd-rich secondary phases and impurities are visible as the areas of bright contrast. Note that cracks have a tendency to develop along the grain interfaces.

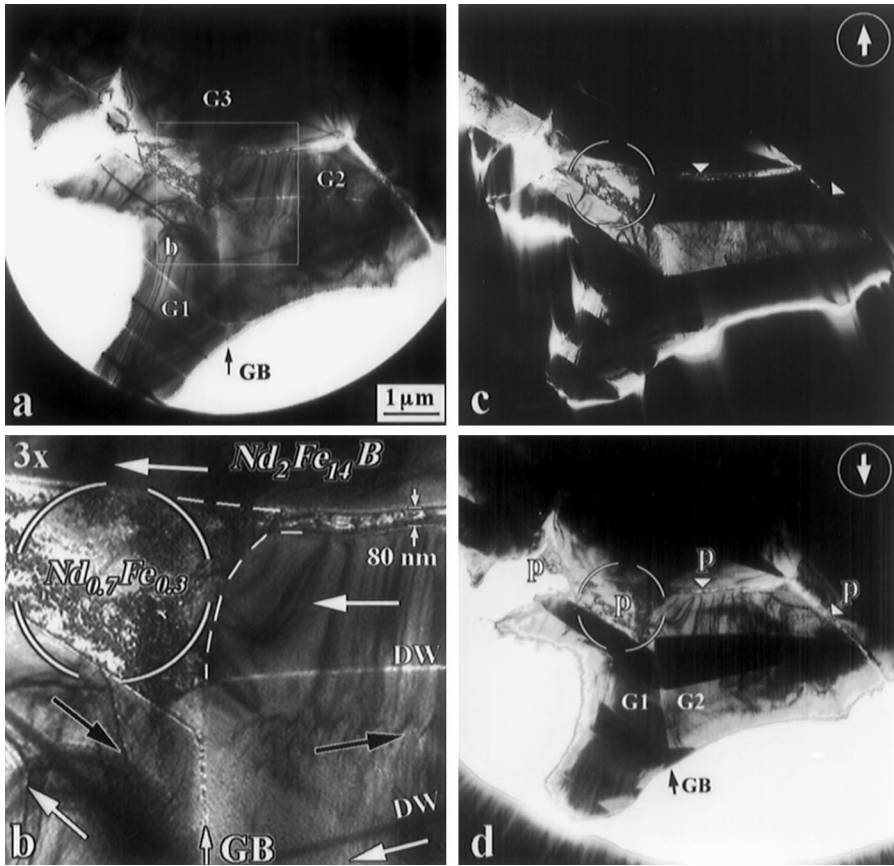


Fig. 2. Magnetic sensitive images of sintered magnet in Fresnel (a,b) and Foucault (c,d) imaging modes. Image (b) is the enlarged box area of the image (a). Here, the arrows show the direction of local magnetization of the domains separated by 180° -domain walls (DW). The non-magnetic 'pocket phase' Nd_7Fe_3 is visible in encircled area in (b)–(d) images; p-letters in image (c) show the presence of the same 'pocket phase' at the GB-interfaces. Here encircled arrows show the direction of the objective aperture shift. Note that coupled 'grain cluster' $G_1 + G_2$ appears to be demagnetized while the whole SI-magnet remains under remanent magnetization.

appear as bright regions with significant difference in their sizes. On the other hand, the Fresnel–Foucault TEM imaging of the cross-sectioned SI-samples (Fig. 2) directly revealed the admixture of 'pocket-phase' approximated by the eutectic composition of Nd_7Fe_3 . The absence of ferromagnetic properties of this grain boundary (GB) phase follows directly from the comparison of complementary Foucault images shown in Figs. 2c and d. Here the encircled area of 'pocket phase' does not follow the inversion of magnetic domain contrast in Figs. 2c and d, because the Lorentz force, deflecting the electron beam inside of mag-

netic domains, is absent for this area and, hence, the magnetic induction of this 'phase' equals to zero/magnet produced by Sumitomo Special Metal Inc.

The degree of preferential alignment of domain walls (DW) in the SI-magnet is a microstructure-sensitive parameter. It is a function of grain size and grain texturing of the 2–14–1 phase. Fig. 2 shows the example of reasonably good magnetic alignment of G_1/G_2 grains coupled into the 'grain cluster' G_1/G_2 , which in turn is magnetically decoupled from the rest of SI-magnet sample by the GB 'pocket phase' (the GB-phase image in Fig. 2d

is traced by p-labels). Note that in many cases the grains within such ‘grain clusters’ are well aligned and coupled without visible presence of secondary GB-phase. Therefore, the preferential orientation of submicron-size strip-like magnetic domains simply follows the local c -axis directions of such grains without interruption at the GB interfaces inside the ‘grain clusters’ (Fig. 2b).

It is important to note that observation of ‘grain clusters’ (GC) formation seems to be valid for more common case. For instance, in averaged much less of grain/domain alignment was found for another SI sample (Fig. 3) (Magnet produced at Carnegie Mellon University). Here Foucault images were taken from SI sample in a demagnetized state. Fig. 3a shows a plan-view image of SI-magnet with a ‘maze’ pattern of the magnetic domains, which corresponds to the grain clusters with c -axis aligned mainly perpendicular to the image plane. Fig. 3b shows a cross-section image of the same SI-magnet. Here the ‘grain clusters’ (G_1 and G_2) are viewed when the major component of their c -axis is projected to the image plane. Note that despite of much worse general alignment of these

GCs, the grain alignment inside of these clusters remains fairly good (like G_1 -grain cluster, Fig. 3b), as well as no visible traces of GB-phase was observed for internal GC-interfaces. This conclusion is consistent with the GC-microstructure observations made for superior quality SI-magnet (Fig. 2) discussed above.

The second type of DU-magnet samples we studied, are characterized by the presence of a well-developed platelet-like fine grain texture (Fig. 4) with a preferential grain orientation of c -axis along the die-upset direction (hot-press direction). The grain sizes did not exceed $0.15 \times 0.6 \mu\text{m}^2$ when viewed along a direction perpendicular to the press direction. Here, the dimension represents the cross section of the platelet-like grains. Most of the small grains are stacked together such that their flat facets (a - b planes) are aligned predominantly perpendicular to the die-upset direction (Fig. 4, A-area) which lies parallel to the averaged c -axis. These platelet-like grains usually have pure twist, or nearly pure twist interfaces between them with common c -axis, which are often free from interfacial GB-phase. The absence of

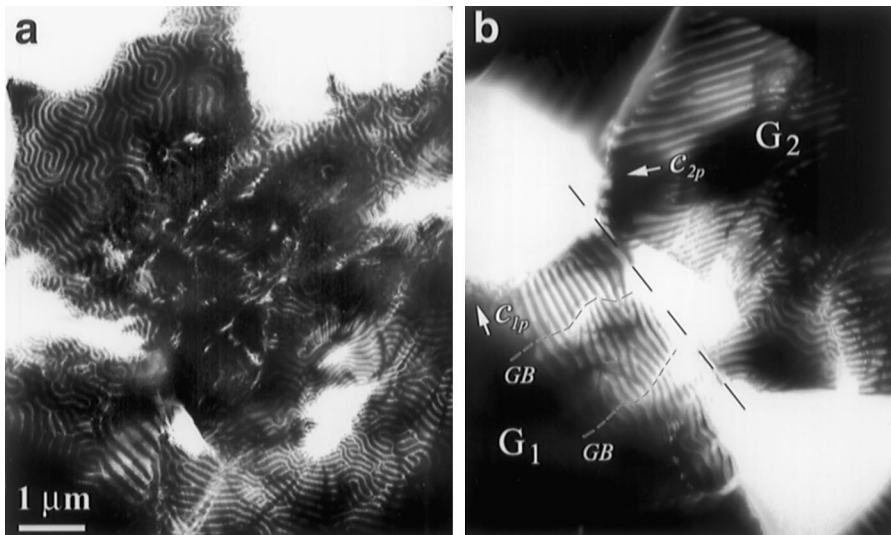


Fig. 3. Foucault images of the SI sample in a demagnetized state: (a) Plan-view image with a ‘maze’ pattern of magnetic domains from the grain clusters with c -axis aligned close to the viewing direction; (b) cross-section image of domain structure for the same SI-magnet. Here the ‘grain clusters’ (G_1 and G_2) are viewed when the major component of their c -axis is projected to the image plane. Note that despite of strong misalignment between these grain clusters, the grain alignment inside the clusters remains fairly good.



Fig. 4. Bright field image of the cross-section sample of the DU-magnet. A good grain alignment in A-areas and absence of such alignment in B-area are clearly visible. The A-area consists of well-aligned platelet-like grains of 2–14-1 phase. Within B-area such alignment is destroyed. It contains a high density of secondary precipitates of ‘pocket-phase’ (marked with p-letters) as well, which may form periodical ‘defect’ layers transverse to die-upset direction (marked with c-arrow) in DU-magnet. The presence of ‘defect’ layers is associated with the flake interfaces originating from Nd–Fe–B ribbons used for form DU-magnets.

grain alignment is visible within ‘defect’ layers (Fig. 4, B-area) which have, in general, a high density of secondary phase precipitates. These ‘defect’ layers are associated with the former flake interfaces originated from Nd–Fe–B ribbons used for form DU-magnets [6]. Our magnetic-sensitive domain images indicate that small well-oriented grains are well coupled into bigger clusters by ferromagnetic exchange interactions. Therefore, they form large ‘interacting’ domains, running across several small grains along their common *c*-axis as a common easy magnetization direction (Fig. 5). We note that the thickness of these grains does not exceed a critical single-domain grain size (D_c), estimated to be about 0.2 [11] or 0.3 μm [12] for the $\text{Nd}_2\text{Fe}_{14}\text{B}$ phase. In the demagnetized state of the anisotropic magnet, the domain clusters with one preferential magnetic direction, say positive, are self-compensated by domain clusters with opposite (negative) magnetization in such a way that the total magnetization remains zero. It is clear that this kind of

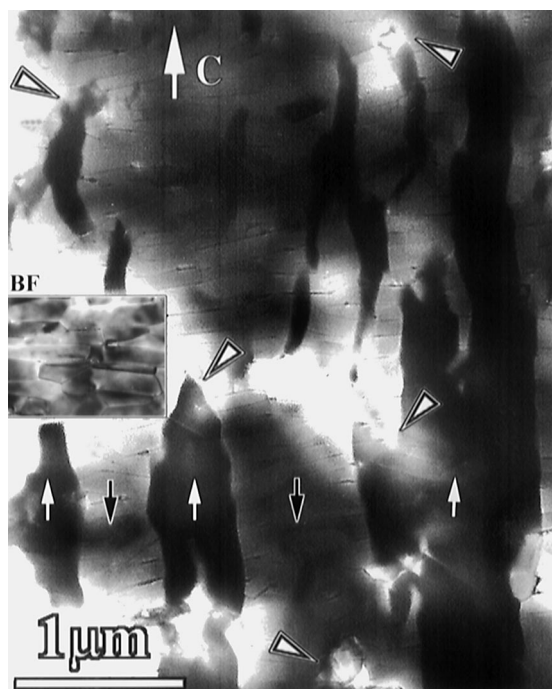


Fig. 5. Large ‘interacting/cluster’ domains in DU-magnet, running across the small platelet-like grains along their common *c*-axis as easy magnetization direction, are shown in this magnetic-sensitive Foucault image. The ‘interacting’ domains of opposite magnetization are painted in black and white colors. Small arrows show the direction of magnetic induction within each domain. Note that the tips of magnetic domains are often pinned by some local imperfections (marked with arrowheads) of the grain texture. The inset shows a conventional bright field (BF) image of the DU-magnet.

microstructure with well-aligned magnetic ‘interacting’ (or cluster) domains will directly contribute to the high remanence of the DU-magnet (Fig. 6), as discussed in the next section. The local defects and extended ‘defect’ layers, as shown in Figs. 5 and 4, respectively, may act as the effective pinning centers for domain walls motion [6], that separate cluster domains with opposite magnetization in the DU-magnet. Nevertheless, not all of the platelet grains fit well, one to another, with their flat facets. Some of them are mixed with precipitates or separated by relatively thick layers (about 30 nm or more) of intergrainular nonmagnetic ‘pocket phase’ as demonstrated from the bright field TEM-image at medium magnification (Fig. 4). The composition of

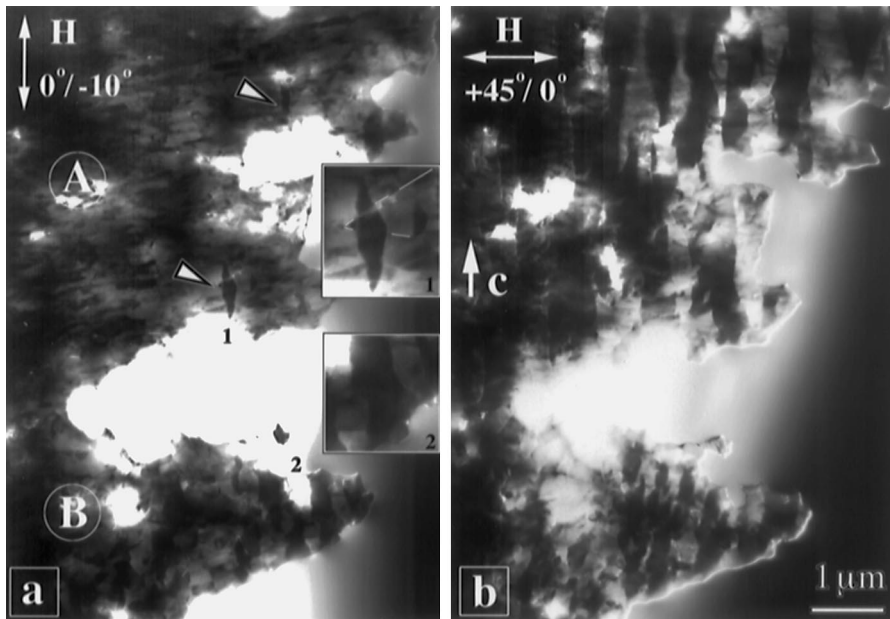


Fig. 6. Foucault images of domain structure for the same area in DU-magnet displayed in remanent magnetization state after in situ saturation with the in-plane component of an external magnetic field applied along the easy (a) and hard (b) magnetic axes by properly tilting the specimen at 10–45°. The A-area, composed of well-aligned grains, remains magnetically saturates in remanence (a), whereas B-area remains unsaturated (defect layer). The insets in (a) show some small not vanished reversal domains in this area.

such a ‘pocket phase’ was determined to be about Nd_7Fe_3 by EDS analysis, which is consistent with the observations of Mishra [13,14]. We will show later that such ‘pocket phase’ may play a key role in forming strong pinning centers in the DU-magnets. High-magnification images clearly show that some of the large-angle grain boundaries between the grain facets consist of a spacer-like intergranular phase with thickness less than 2 nm. Such intergranular phase was found to be Fe-rich [15], however, their pinning effect remains unclear.

3.2. In situ TEM magnetizing experiments

For fairly large crystalline grains of 1–4 μm , which exceed the single-domain grain size $D_c = 0.2\text{--}0.3\ \mu\text{m}$, a multi-domain configuration exists in the demagnetized state of the SI-magnets. Each grain consisted of several ferromagnetic domains separated by equidistant domain-walls, presumably 180° Bloch walls, with antiparallel aligned magnetized moments for each domain. We note

that the equilibrium domain width (D) of different grains in the SI-magnet varied over a surprisingly wide range $D = 0.07\text{--}0.9\ \mu\text{m}$. In the case of demagnetized DU-magnet samples, large cluster domains approximately 0.4–0.6 μm wide were observed by Lorentz microscopy. In most cases, their length was limited by the extended ‘defect’ layers (B layers in Fig. 4) or by local defects, which serve as pinning (or nucleating) centers of reversed domains, as shown in Fig. 5. It is difficult to differentiate experimentally between the nucleation and pinning nature of the structural defects based on the ‘static’ magnetic images. Only dynamic magnetizing experiments combined with Lorentz imaging can help to identify the nature of such centers.

3.2.1. Die-upset magnets

Figs. 6a and b show two Foucault images taken in the remanent state from the same area of a DU-magnet, magnetized along the easy and hard magnetic directions, respectively (with applied field $\mu_0 H \approx 2\ \text{T}$). The in-plane magnetizing component

of the field was proportional to the projection of the tilt angle given in the images. The drastic change in local remanence with the direction of the applied field is very clear, and can be quantitatively measured from the ratio of the black (D_u) to white (D_d) regions, i.e., magnetic domains with opposite magnetization. Indeed, the width ratio D_u/D_d for opposite domains, very close to unity, is clearly visible in Foucault image of Fig. 6b. This strongly suggests that the $B_{r,\perp}$ component of the remanence B_r and magnetic hysteresis must be small along the hard magnetic plane in anisotropic Nd–Fe–B DU-magnets. On the other hand, a well-aligned grain region (A-area in Fig. 6a) remains well saturated when the external field, applied along the easy axes, was

removed. Meanwhile, the ‘defect-layer’ (B-area in Fig. 6a) is far from such saturation. Hence, only aligned grains directly contribute to the high remanence of the DU-magnet ($B_{r,\parallel} \approx B_s$ in A-area), whereas in the non-aligned grains (B-area in Fig. 6) the associated domains essentially cancel each other out in the absence of magnetic field. It is clear from these data that a higher local remanence of the DU-magnet can be reached only along the die-upset direction, even with a smaller magnetic field applied.

A few very small reversal domains were observed in A-area marked by arrowhead-1 (see inset 1, Fig. 6a). Their presence is controlled by local imperfections, such as inclusions or misalignment of grains.

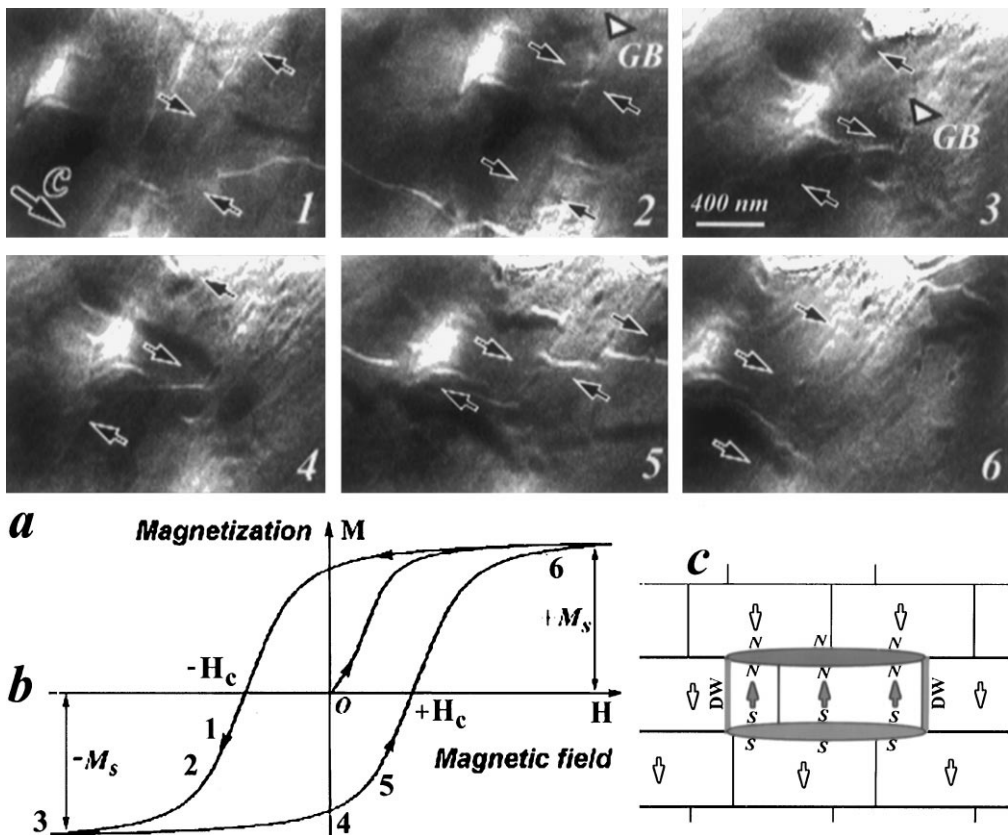


Fig. 7. Successive Fresnel images (a: 1–6) of local domain structure evolution in a DU-magnet at different points of magnetization loop (b: 1–6). The evidence of strong pinning center, not vanished under the strong in-plane negative field $(H_{\parallel})_{\min} < -H_c$, is given in the images (a: 3), (b: 3) and estimated as $\mu_0(H_{\parallel})_{\min} \approx -1$ T (see text for details). A simple structure model of the pinning center (c) shows how the domain of opposite magnetization is trapped by the low-energy defect formed by the grains decoupled magnetically from the outer area by a pair of thick non-magnetic GB-layers and domain walls (DW).

In the latter case, the shape of the reversal domain was found to be sensitive to the angle of grain misalignment. In situ TEM magnetizing experiments confirmed that such small reversal (or negative) domains, associated with non-aligned grains, continue to grow slowly under the increasing negative field until they nucleate a *c*-axis aligned reversal domains at the nearest GBs. Starting from this point magnetization reversal transforms rapidly to an irreversible process. Such domains, in turn, can easily propagate through the area of well-aligned grains in a negative field exceeding some critical value H_{loc} , as clearly demonstrated in Fig. 7 by series of successive images captured from video recording. Once the reversal domain is nucleated, only the pinning of the domain walls at GBs (Fig. 7) controls its further expansion. Thus, the leading mechanism in controlling the magnetization reversal seems to be the nucleation of reversal domains, preferentially at misaligned grain interfaces or sample surfaces where the demagnetizing field is the largest [1]. Frame-3 in Fig. 7a shows the example of a ‘double-GB’ strong pinning center, where the domain trapped by the GBs remains positively magnetized under the extreme negative applied field $H < -H_c$ (Fig. 7b). This center was found to be responsible for the nucleation of positive domains at $H \approx +H_c$ for the 4th quadrant of hysteresis loop (frames 4–6 of Fig. 7a), starting from negative magnetization. Fig. 7c is a schematic structural model of such a ‘double-GB’ pinning center. In this model a single-domain grain with an opposite magnetization with respect to the matrix is uncoupled along the easy magnetic direction due to thick non-magnetic layer or ‘pocket phase’ at its double GBs. The presence of non-magnetic or ‘pocket phase’ at the GBs is the necessary condition for the ‘pinning’ by such a defect center. It reduces a high density of magnetic charges (Fig. 7c) by spreading them around this GB-buffer layer. Our observations are consistent with the well-known experimental trend of the strong dependence of the coercive field $H_c(H_{max})$ on the maximum applied field used to saturate the magnet. The higher the saturation field (H_{max}) is, the higher the coercive field H_c can be reached. Such behavior of $H_c(H_{max})$ indicates that a stronger field can gradually

remove the nuclei of reversed domains existing at such GBs. However, in our experiments the in-specimen plane component of the projected field $((B_{\parallel})_{max} = \mu_0 H \sin 30^\circ \approx 1.0 \text{ T})$ was not sufficient to reach saturation of the coercivity.

3.2.2. Sintered magnets

Our in situ TEM experiments on SI-magnets revealed that at the early stage of magnetization reversal a new reversible process starts to develop, as shown in a set of still images (Fig. 8a) captured from a videotape. We shall call this ‘dipole domain’ (DD) motion. It reveals how narrow dipole-like domains of negative magnetization start to expand and grow in the interiors of the grain when the applied field decreases slowly from positive saturation. We note that the grains with *c*-axis tilted away from the applied field direction are more likely to form reversal ‘dipole domains’. When the applied field decreases the dipole domains tend to align more closely to the *c*-axis of the grains because this reduces the energy of domain walls. A schematic drawing of the DD-motion is shown in Fig. 8b. The dipole domain can be imagined as a pair of ordinary reversal domains, enclosed one into another. In this case the total area of a dipole domain, sandwiched between two parallel domain walls and magnetized opposite to that of the matrix, remains very narrow. Such a dipole domain may only slightly change the local magnetization. On the other hand, it serves for easy and almost reversible motion for the ‘coupled’ domain walls, since their movement in DD-configuration requires a lower critical field for magnetostatic energy in comparison with traditional single-domain motion (Fig. 8c). The magnetic charges, or the N/S-poles, are magnetostatically coupled at the reverse DD tips and remain unchanged on such a motion (Fig. 8b), until they reach the GBs.

When the applied field decreases further and becomes negative, the major irreversible demagnetization mechanism comes into the play (Fig. 9). The corresponding process takes place usually at the GBs, where the nucleation of reversal (negative) domains occurs via nucleation and several sudden splittings of positive domains. The nucleation transforms a positive domain into a

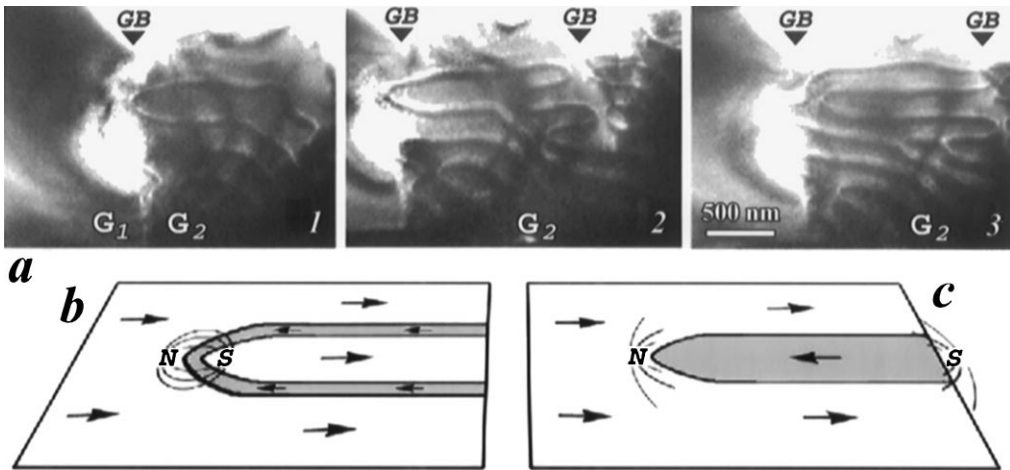


Fig. 8. A set of Fresnel images (a), captured from video, shows the expansion of dipole-like domains in SI-magnet under decreasing magnetic field. A simple model of such dipole domain (b) is compared with the ordinary magnetic domain (c). Note that dipole domain requires lower critical field of magnetostatic energy.

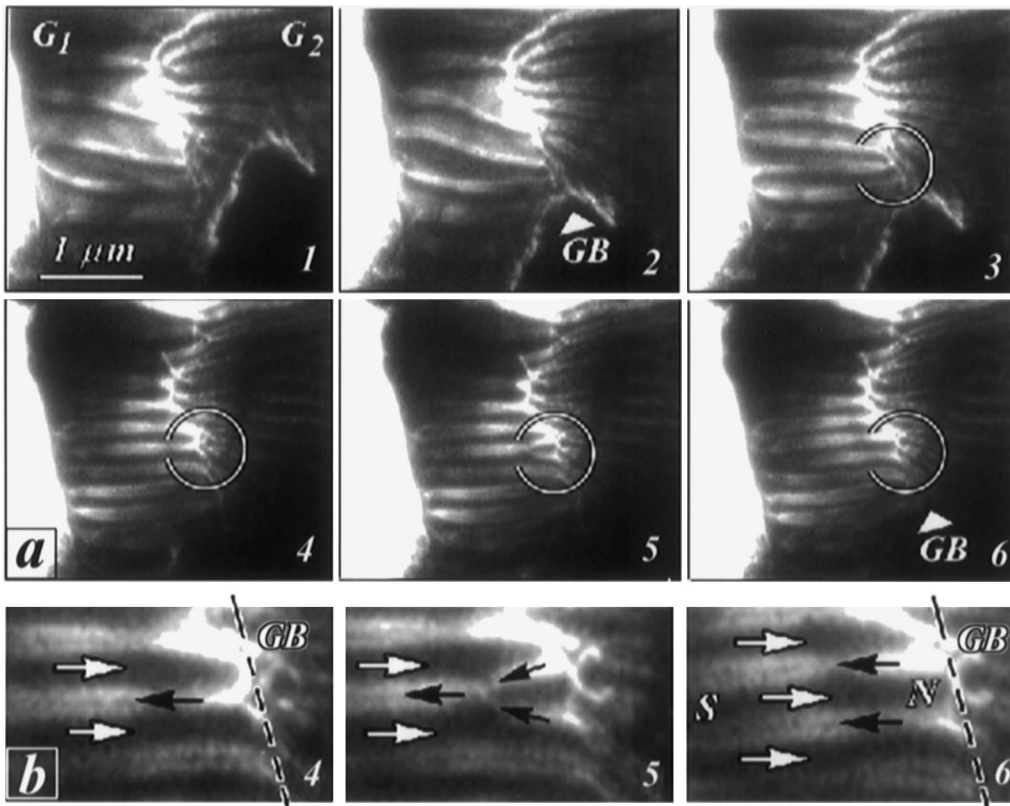


Fig. 9. Successive Fresnel images (a: 1–6), captured from videotape, show the in situ irreversible remagnetization process in SI magnet under decreasing magnetic field. It occurs by the nucleation of new domains marked with black arrows in (a: 4–6) via splitting of single domains of the same magnetization near the grain boundary (GB) as shown in the enlarged images (b: 4–6).

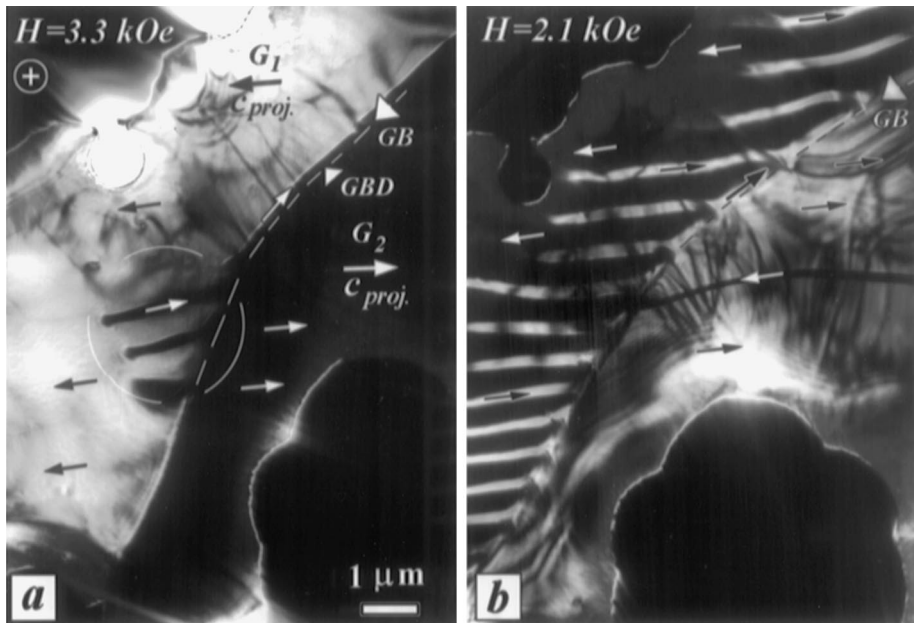


Fig. 10. Foucault images (a,b) of the same GB-area under decreasing magnetic field. Nucleation (a) and expansion (b) of reverse magnetic domains in the grain G_1 occur via the formation of specific 'grain boundary' domain (GBD), which lowers the local magnetic anisotropy along the GB-line (a). Here the GB is traced by the dashed line and local in-plane direction of magnetization for magnetic domains in (a,b) is shown by the fine arrows. They are opposite for G_1/G_2 grains as follows from the black/white contrast of these domains. Indeed, SAED pattern analysis confirmed that G_1/G_2 grains have parallel in-plane c -axis components (c_{proj}) and enclose a misorientation angle about 84° .

positive–negative–positive domain configuration, enclosing a pair of newly generated 180° -domain walls. This process is essentially irreversible and may be considered as cascade-like discharge of oversaturation of magnetic charge (or poles) at the GB. The formation of reversal domains through this process reduces the magnetostatic energy of each GB by self-compensating the newly created N/S-poles at the GB. The process is completed with lateral expansion of newly created domain walls.

It is interesting to note that in the case of wavy grain boundaries with a large GB misorientation, an additional the so-called 'grain boundary magnetic domain' was found to nucleate along the GB (Fig. 10a). Its local magnetization direction is determined by the position of the GB plane, and does not follow any easy magnetic axis of the grains separated by such a GB. Therefore, it reduces the local GB-anisotropy. The width of such GB-domain was found to be field-sensitive and did not exceed 100 nm. It is clear that the presence of

a GB-domain eases magnetization reversal through the GB at low fields (Fig. 10b). We assume that such GB-domains can lower the density of magnetic charges at the GB through the nucleation of magnetic domain and its expanding along the boundary (Fig. 10b) at lower magnetic field. Thus, this process is somewhat similar to nucleation of Néel spike domains which occur near the holes in some other ferromagnetic materials. Note that prior to study the SI-magnet, shown in Fig. 10, it was subjected to prolonged annealing at 750°C , which resulted in drastic decrease of its averaged coercive force down to $H_c = 0.3$ kOe. Therefore, the in situ remagnetization process, shown in Fig. 10, is a case study of 'strong GB-pinning', which is expected to occur only for GB-interfaces with a high degree of c -axis grain misorientation. Indeed, SAED and Kikuchi pattern analysis confirmed that c -axis of G_1/G_2 grains enclose an angle of 84° and are parallel when projected to the image plane (arrows c_{proj}) in Fig. 10.

4. Discussion

We have demonstrated that many of the magnetic properties sensitive to microstructure of hard SI- and DU-magnets can be well explained based on our TEM observations of the evolution of domain structure imaged in real time by the Lorentz microscopy methods, both in Fresnel and Foucault modes. Our analysis and interpretation of the magnetic structure are consistent with the observed microstructure of hard magnets using conventional TEM methods including selected area electron micro-diffraction (SAED) and X-ray spectroscopy (EDS). Despite very big differences in microstructure between the two types of magnetic samples, there are some remarkable common features in the behavior of their magnetic domain structures. First, both SI- and DU-Nd-Fe-B magnets display a certain *c*-axis-oriented grain texture with preferential *c*-axis grain alignment along the common easy magnetic axis. This feature explains the anisotropy effect of the hard magnets: high remanence of the magnets along the easy axis, and low remanence in the basal plane. We note that our conclusion on grain alignment in SI-samples was less evident since only a limited number of observations were used in our statistical analysis. Another common feature of these magnets is that both may form big cluster domains coupled inside by the ferromagnetic exchange interaction. In the case of DU-magnets, these are known as ‘interacting’ domains, consisting of many small, well-aligned ferromagnetically coupled grains. In SI-magnets such clusters may be formed by a few large coupled grains, separated from other similar clusters by thick intergranular non-magnetic phases. Such a cluster description may be useful for explaining their similar magnetic properties and shape of the second quadrant of the hysteresis curve for DU- and SI-samples. If we assume that magnetization reversal in both cases occurs via the non-uniform reversal of such cluster domains, then the difference in their microstructure may not be important as long as magnetically coupled cluster domains are formed. However, this secondary process would occur only when the primary process of nucleation of small reversal domains in clusters is completed. Therefore, this

process can help to increase the coercive field, which is mainly controlled by the primary nucleation mechanisms.

5. Conclusion

In situ magnetizing experiments combined with Fresnel–Foucault modes of Lorentz microscopy are very useful to address the magnetization reversal in polycrystalline anisotropic magnetic materials. A small excess of Nd over the stoichiometry of Nd₂Fe₁₄B hard phase in SI- and DU-magnets plays an important role in determining their magnetic behavior. Our TEM observations suggest the presence of an additional non-magnetic Nd-rich ‘pocket phase’ approximated with eutectic composition Nd₇Fe₃, which is responsible for magnetic decoupling of cluster domains and, therefore, increases indirectly the coercive force. Although the behaviors of the hysteresis curves *I*(*H*) of DU- and SI-magnets are similar, their nanoscale magnetization reversal was found to be controlled by different mechanisms. Nucleation of reversed domains, preferentially at misaligned grains on the grain interfaces and sample surface, where the demagnetizing field is the largest, followed by domain walls pinning at the grain boundaries, is likely to be the leading mechanism in controlling the remagnetization process in DU-magnet. On the other hand, magnetization reversal in SI-magnet was found to occur in successive steps — by nucleation and expansion of reversal dipole domains in a positive magnetic field and then by the major nucleation process of reverse domains via splitting of magnetic domains near the GBs in a more negative field. Here, the first mechanism provides a relatively easy and reversible expansion of domain walls through the magnetized grains. The irreversible magnetization is associated with the second mechanism, i.e. splitting of domains at the grain boundaries.

Acknowledgements

This research was supported by the US Department of Energy, Division of Materials, Office of

Basic Energy Science, under the Contract No. DE-AC02-98CH10886.

References

- [1] H. Kronmuller, in: G.C. Hadjipanayis, G.A. Prinz (Eds.), *Science and Technology of Nanostructured Materials*, NATO ASI Ser. B, Physics, Vol. 259, Plenum Press, New York, 1991, p. 657.
- [2] D. Givord, Q. Li, M.F. Rossignol, in: G.C. Hadjipanayis, G.A. Prinz (Eds.), *Science and Technology of Nanostructured Materials*, NATO ASI Ser. B, Physics, Vol. 259, Plenum Press, New York, 1991, p. 635.
- [3] R.W. Lee, *Appl. Phys. Lett.* 46 (1985) 790.
- [4] R.W. Lee, E.G. Brewer, N.A. Schaffel, *IEEE Trans. Magn.* MAG-21 (1985) 1958.
- [5] C.D. Fuerst, E.G. Brewer, *J. Appl. Phys.* 73 (1993) 5751.
- [6] V.V. Volkov, Y. Zhu, *J. Appl. Phys.* 85 (1999) 3254.
- [7] M. Sagawa, S. Fujimura, N. Togawa, H. Yamamoto, Y. Matsuura, *J. Appl. Phys.* 55 (1984) 2083.
- [8] J. Hu, Y. Liu, M. Yin, Y. Wang, B. Hu, Z. Wang, *J. Alloys Compounds* 288 (1999) 226.
- [9] V.V. Volkov, D.C. Crew, Y. Zhu, L.H. Lewis, *Proceedings of the Conference on Microscopy and Microanalysis*, Vol. 5 (Suppl. 2) Portland, Oregon, August 1–5, 1999, pp. 46–47.
- [10] V.V. Volkov, Y. Zhu, private communication.
- [11] D.D. Mishin, in: *Magnetic Materials*, High School, Moscow, 1991, 284 (in Russian).
- [12] J.F. Herbst, *Rev. Mod. Phys.* 63 (1991) 819.
- [13] R.K. Mishra, *J. Appl. Phys.* 62 (1987) 967.
- [14] R.K. Mishra, *Mater. Sci. Eng. B* 7 (1991) 297.
- [15] Y. Zhu, J. Taftø, L.H. Lewis, D.O. Welch, *Philos. Magn. Lett.* 71 (1995) 297.